# Plastic deformation of pentagonal silver nanowires: Comparison between AFM nanoindentation and atomistic simulations

Marcel Lucas,[1] Austin M. Leach,[2] Matthew T. McDowell,[2] Simona E. Hunyadi,[3] Ken Gall,[4,*]
Catherine J. Murphy,[3] and Elisa Riedo[1,†]

[1]*School of Physics, Georgia Institute of Technology, Atlanta, Georgia 30332-0430, USA*
[2]*School of Materials Science and Engineering, Georgia Institute of Technology, Atlanta, Georgia 30332-0245, USA*
[3]*Department of Chemistry and Biochemistry, University of South Carolina, Columbia, South Carolina 29208, USA*
[4]*School of Materials Science and Engineering and George Woodruff School of Mechanical Engineering, Georgia Institute of Technology,*
*Atlanta, Georgia 30332-0245, USA*

The plastic deformation of a pentagonal silver nanowire is studied by nanoindentation using an atomic force microscope (AFM). AFM images of the residual indent reveal the formation of a neck and surface atomic steps. To study the microscopic deformation mechanism, the indentation force-depth curve is converted to an indentation stress-strain curve and compared to the tensile stress-strain curves predicted by the atomistic simulations of pentagonal silver nanowires. The indentation stress-strain curve exhibits a series of yielding events, attributed to the nucleation and movement of dislocations. The maximum stress measured during nanoindentation (2 GPa) is comparable to the tensile yield strength predicted by atomistic simulations.

　　　　PACS number(s): 62.25.−g, 62.23.Hj, 68.37.Ps

## I. INTRODUCTION

Due to their high conductivity and aspect ratio, silver nanostructures are potential building blocks for future nano-electromechanical devices and chemical sensors. A wide range of silver nanostructure morphologies has been reported, including wires, particles, cubes, and pyramids, each with distinct electronic and optical properties.[1] Recently, silver nanowires with pentagonal cross sections have been synthesized via different chemical processes and observed by transmission electron microscopy (TEM).[1–4] Atomistic simulations of the tensile deformation behavior of these nanowires have predicted an enhanced mechanical strength, compared with nanowires with rhombic or truncated-rhombic cross sections.[5]

In general, experiments on the plastic deformation of nanostructures under tensile loading are challenging. Direct observation of deformation in nanometer-size gold nanowires by TEM revealed atomic slip steps under tensile stress and twinning under shear stress,[6] but accurate force measurements could not be collected *in situ*. Quantitative force measurements on metallic nanowires (as opposed to nanometer scale compression pillars[7–11]), formed *in situ* through indentation and retraction, have been performed using scanning probe microscopy.[12,13] Wu *et al.*[14] used an AFM tip to bend individual pentagonal silver nanowires suspended over a trench and reported a superelastic behavior followed shortly by failure without significant plastic deformation. An experimental technique more commonly used to study the mechanical properties of nanostructures is nanoindentation, which represents a useful solution for nanostructures, brittle materials, or thin films.[15] Nanoindentation studies on silver nanowires have focused mainly on the elastic properties, particularly the size dependence of the Young's modulus.[16,17] Nanoindentation studies on the plastic deformation of nanowires have only consisted of the determination of their hardness.[16]

Most theoretical studies pertaining to the plastic deformation of individual metal nanowires consider nanowires under axial loading,[18–20] and they involve nanowires with a diameter much smaller than 5 nm, below the typical size of chemically grown nanowires, making the comparison between theory and experiments difficult. Efforts to convert indentation force-depth curves to stress-strain curves, which could be comparable to typical stress-strain curves from tensile tests, were attempted on metals such as copper and steel.[21] Field and Swain[22] proposed a method to extract the stress-strain curves from submicrometer indentation tests, which was further developed to obtain the Young's modulus and yield strength of a wide range of materials.[23–25] The same approach was also successful in the study of plastic deformation mechanism in GaN thin films[26] and mica.[27] However, this method has been applied only to bulk materials and thin films.

In this report, the plastic deformation of a pentagonal silver nanowire is studied experimentally by nanoindentation using an atomic force microscope (AFM). The AFM enables the accurate force measurement and subsequent observation of the residual indent with nanometer scale resolution. AFM images of the residual indent reveal the formation of a neck and surface atomic steps. The loading indentation force-depth curve is converted to an indentation stress-strain curve and compared to the tensile stress-strain curves predicted in atomistic simulations of pentagonal silver nanowires.

## II. EXPERIMENT AND COMPUTATIONAL METHODS

The silver nanowires were prepared in water by a seedless and surfactantless wet chemical process as previously described.[2] Electron-diffraction patterns confirmed that these nanowires are not single crystals but twinned, such as with a fivefold twinned crystal structure and pentagonal cross section.[1–4] A droplet of the solution was deposited on an oxidized silicon wafer and left to dry for an hour in the dark

before the AFM measurements. AFM images showed that the height (diameter) of the nanowires laying on the substrate surface ranged from 15 to 40 nm.

The nanoindentation data were collected using a Veeco CP-II AFM with a silicon tip (RTESP, Veeco) at room temperature and in air. AFM topography images were collected before and after the nanoindentation test with the same tip in the tapping mode. The normal cantilever spring constant, 46 N/m, was calibrated using the method of Sader *et al.*[28] The normal force was calibrated by recording the deflection of the cantilever as a function of the scanner displacement while in contact with the silicon substrate. AFM images were used to locate the nanowire and position the tip over the middle of the nanowire to collect the force-depth curve. The total data acquisition time (loading and unloading) during which the tip was in contact with the nanowire was about 0.6 s.

The loading force-depth curve was converted to an indentation stress-strain curve by extending the approach described by Basu *et al.*[23] to inelastic displacements. The indentation stress is obtained by dividing each force value by the corresponding instantaneous contact area. The contact area is estimated by considering a perfectly spherical tip indenting a pentagonal nanowire that has ideal plastic deformation behavior. At a particular indent depth, the contact area is defined as the projected area of the section of the tip that penetrated the pentagonal nanowire. From the apparent width of the nanowire on AFM images, the AFM tip radius is estimated to be 60 nm, a value that is consistent with the one measured by imaging a silicon calibration grating TGT01 (MikroMasch, Tallinn, Estonia). The indentation strain is defined as the ratio between the instantaneous contact radius and the tip radius. The contact radius is the radius of the equivalent circle of contact delimiting the contact area. Although more sophisticated methods exist for calculating indentation stress and strain, these methods typically assume flat indentation surfaces. In the current situation, the indentation stress and strain are calculated for a tip penetrating a pentagonal surface; as such, they represent crude approximations of contact area, contact stress, and contact strain.

The simulations in this work were performed using molecular dynamics (MD) with the embedded atom method (EAM).[5,29,30] The semiempirical EAM potential for silver developed by Voter and Chen[31] was utilized. This potential is fit to a number of experimentally determined parameters of bulk silver, including the equilibrium lattice constant, bulk cohesive energy, bulk modulus, vacancy formation energy, cubic elastic constants, and diatomic molecule bond strength and bond length. The nanowires tested were created with atoms in positions corresponding to a bulk face-centered-cubic crystal lattice, with a pentagonal cross section. The nanowires have {100} lateral surfaces and are axially oriented along the ⟨110⟩ direction; periodic boundary conditions were not imposed in any direction. Two different-sized nanowires were tested in the simulations to determine the effect of nanowire size on surface step behavior during deformation. The first nanowire was made up of 854 135 atoms and was 89.3 nm long and 15.24 nm thick, and the second was made up of 64 883 atoms and was 38.07 nm long and 6.3 nm thick. The nanowires underwent conjugate gradient energy minimi-
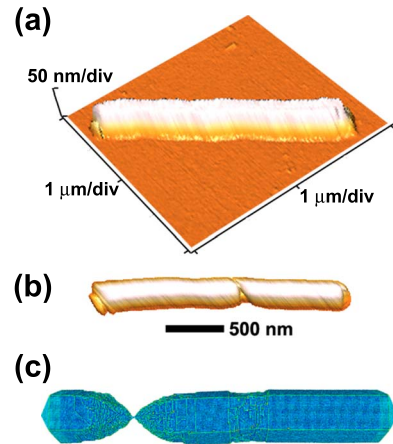


FIG. 1. (Color online) AFM images ($2 \times 2$ $\mu m^2$) of a silver nanowire (a) before and (b) after the nanoindentation test (top view). (c) Atomistic simulation of a pentagonal silver nanowire of diameter 15 nm under tensile stress.

zation to achieve a state of static equilibrium and were then dynamically equilibrated at 300 K using a Nose–Hoover thermostat for 100 ps. After this step, a tensile displacement-controlled load was applied until failure. The loading method consisted of assigning each atom a displacement in the axial direction according to a linearly varying displacement profile along the nanowire length. After each displacement, the ends of the wire were constrained from axial motion and the wire was dynamically equilibrated at 300 K for 100 ps. This allowed for relaxation of the strain in the nanowire perpendicular to the axial direction while maintaining the externally imposed load in the axial direction. The effective strain rate was $10^8$ $s^{-1}$. The stress in the nanowire was calculated using the virial theorem and averaged over the instantaneous volume of the nanowire.[32,33]

## III. RESULTS AND DISCUSSION

The AFM image in Fig. 1(a) shows a silver nanowire, which is about 2 $\mu m$ long and 40 nm high. The top surface of the nanowire is smooth and does not present any detectable defects. The AFM tip was positioned over the middle of the nanowire to perform the nanoindentation test. The AFM image after the indent shows limited pile-up on both sides of the indent: the nanowire surface is elevated by less than 1.5 nm, over a length of about 200 nm on each side [Fig. 1(b)]. The nanowire remained straight after the test and did not move, suggesting that the adhesion forces between the nanowire and the substrate were strong enough to prevent it from rolling or being dragged during the nanoindentation test and the scan after the test. An image of the fracture site confirms the presence of a neck, i.e., the indented area is actually narrower than the original section of the nanowire [Figs. 2(a) and 2(b)]. Similar necks were observed after the nanoindentation of other silver nanowires on the same sample (data not shown). A typical height profile across the nanowire more than 100 nm away from the fracture site [line L1 in Fig. 2(b)] shows a relatively smooth nanowire surface. A height profile across the nanowire in the middle of the indent reveals a
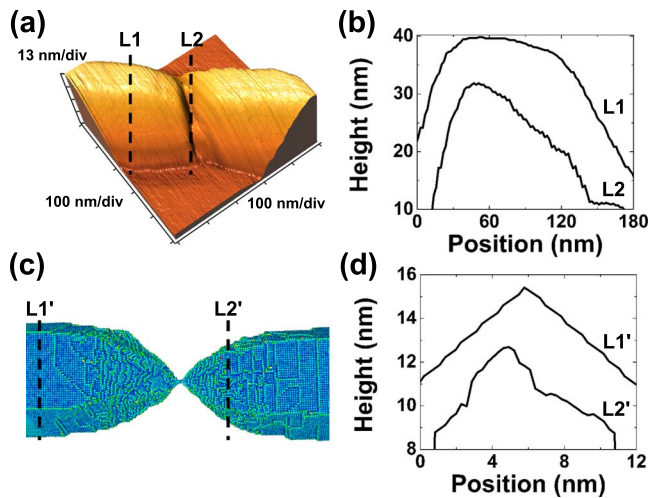
FIG. 2. (Color online) (a) AFM image ($500 \times 500$ nm$^2$) of the silver nanowire after the nanoindentation test and (b) height profiles across the nanowire about 200 nm away from the fracture site ($L1$) and at the fracture site ($L2$). (c) Atomistic simulation of a pentagonal silver nanowire of diameter 15 nm under tensile stress before fracture. (d) Height profiles across the nanowire about 30 nm away from the smallest section of the neck ($L1'$) and around the neck ($L2'$).

series of atomic steps of height ranging from 0.4 to 2.8 nm [line $L2$ in Fig. 2(b)].

The shape of the indented area is similar to the neck formed during plastic deformation under tensile stress for a nanowire with the same pentagonal structure.[5] In order to compare the plastic deformation behaviors, MD simulations were carried out on a 15 nm thick pentagonal silver nanowire under a tensile load until failure. A snapshot of the nanowire under a tensile strain of 19.2% is shown in Fig. 1(c). It represents the last deformation stage before failure, where the narrowest section of the neck consists of only 6–10 silver atoms [Fig. 2(c)]. A typical height profile across the nanowire more than 20 nm away from the fracture site [line $L1'$ in Fig. 2(d)] shows a smooth nanowire surface. A height profile across the nanowire near the necking section shows a few atomic steps of height ranging from 0.4 to 1.2 nm [line $L2'$ in Fig. 2(d)]. MD simulations of the 6-nm-thick pentagonal silver nanowire also show similar atomic steps around the neck before failure but the smaller size of the neck limits their number and keeps their height below 0.9 nm (data not shown). Therefore, the larger number and greater height of the atomic steps observed on the 40-nm-thick nanowire [Fig. 2(b)] are expected.

From the loading and unloading force-depth curves [Fig. 3(a)], the maximum indent depth is 40 nm, which is equivalent to the height of the nanowire, meaning that the nanowire was completely ruptured after the test. The near-vertical unloading curve indicates that there is essentially no elastic recovery from the silver nanowire. The force-depth curve exhibits a series of discrete yielding events, indicated by sudden displacements with no force variation or small force decreases. These so-called pop-in events were previously observed during the nanoindentation of thin gold films,[34] gold, and tungsten single-crystals.[35,36] For depths below 16 nm,
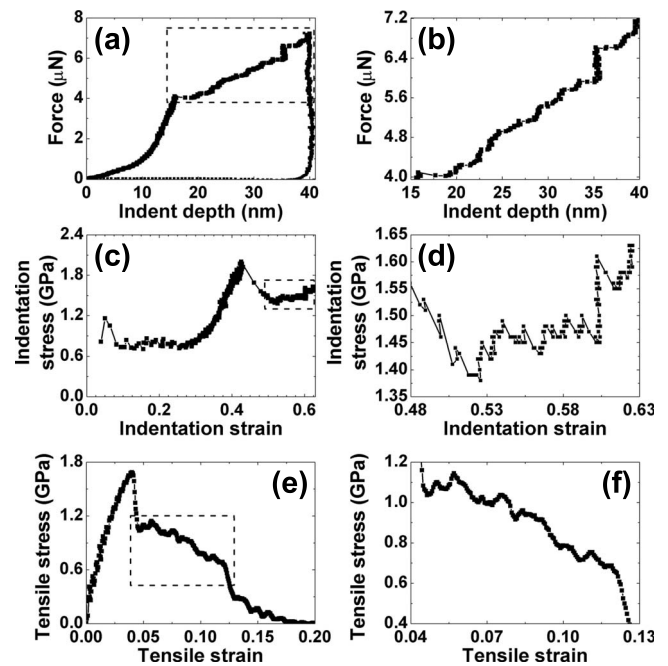


FIG. 3. (a) AFM force-depth loading and unloading curves recorded during the nanoindentation of a silver nanowire of 40 nm diameter. (c) Indentation stress-strain curve obtained from the force-depth loading curve shown in (a). (e) Tensile stress-strain curve of a pentagonal silver nanowire of diameter 15 nm predicted by atomistic simulations. The areas delimited by the dashed lines in (a), (c), and (e) are magnified in (b), (c), and (f), respectively.

only a few pop-in events are observed, since the displacements are smaller than 0.5 nm. At a depth of 16 nm, a sudden displacement of 3 nm was observed and for depths higher than 16 nm, at least 11 more pop-in events occurred with displacements ranging from 0.5 to 2 nm [Fig. 3(b)].

The indentation stress-strain curve calculated from the force-depth curve [Fig. 3(c)] shows a constant indentation stress of about 0.8 GPa for indentation strains below 0.3. At strains between 0.3 and 0.43, the indentation stress increases linearly with strain. At low strains, only a linear elastic behavior is expected; thus the initial stress plateau is probably due to an underestimation of the contact area, since the nanowire is not undergoing full plastic deformation at this point. At a strain of 0.43, the indentation reaches a maximum value of 2 GPa before dropping to 1.4 GPa. This steep drop is followed by a series of yielding events with smaller stress decreases until failure [Fig. 3(d)].

This series of yielding events is similar to that predicted by MD simulations of the nanowire under tensile stress [Figs. 3(e) and 3(f)], which provides insight into the plastic deformation mechanism of the nanowire during nanoindentation. The pentagonal nanowires can be viewed as multishell structures, consisting of stacked layers of silver atoms forming pentagonal shells, with five internal twin boundaries. The 15-nm-thick nanowire deforms elastically up to a strain of about 4%, and the tensile stress increases almost linearly with strain [Fig. 3(e)]. Once the stress reaches the yield strength of 1.7 GPa, plastic deformation is initiated by the fracture of the outer shell, which is accompanied by a

large stress decrease. After this first drop, the atomistic simulations predict a series of dislocation-governed yielding events until failure [Fig. 3(f)]. Each event is characterized by an elongation with little force variation corresponding to the motion of dislocations around the eventual fracture site. Once the dislocation has reached a twin boundary, the stress increases until a fracture occurs at a new location and the stress drops again. The yield strength of the nanowire is expected to decrease with increasing nanowire thickness for thicknesses below 10 nm and remain almost constant for thicknesses above 10 nm.[5] Therefore, the yield strength of a 40-nm-thick nanowire is expected to be close to the yield strength of 1.7 GPa for a 15-nm-thick nanowire, which is in good agreement with the maximum measured indentation stress of 2 GPa. This value is also close to the theoretical ultimate tensile stress, 2 GPa, of a perfect silver crystal under [110] uniaxial loading, predicted by an EAM model that reproduces the empirical values of the second- and third-order elastic constants.[37]

## IV. SUMMARY

In summary, the plastic deformation of a pentagonal silver nanowire was studied by AFM nanoindentation and atomistic simulations. AFM images of the residual indent reveal the formation of a neck and surface atomic steps. Atomistic simulations of a pentagonal silver nanowire under tensile stress also predict the formation of atomic steps of similar height around the neck resulting from the emission of dislocations at the fracture surface. The indentation stress-strain curve exhibits a series of yielding events, corresponding to the nucleation and movement of dislocations predicted by atomistic simulations. The maximum stress measured during nanoindentation (2 GPa) is comparable to the tensile yield strength predicted by atomistic simulations.

## ACKNOWLEDGMENTS

*ken.gall@mse.gatech.edu.

†elisa.riedo@physics.gatech.edu.

[1] B. Wiley, Y. Sun, and Y. Xia, Acc. Chem. Res. **40**, 1067 (2007).

[2] K. K. Caswell, C. M. Bender, and C. J. Murphy, Nano Lett. **3**, 667 (2003).

[3] X. Sun and Y. Li, Adv. Mater. (Weinheim, Ger.) **17**, 2626 (2005).

[4] H. Chen, Y. Gao, H. Zhang, L. Liu, H. Yu, H. Tian, S. Xie, and J. Li, J. Phys. Chem. B **108**, 12038 (2004).

[5] A. M. Leach, M. McDowell, and K. Gall, Adv. Funct. Mater. **17**, 43 (2007).

[6] T. Kizuka, Phys. Rev. B **57**, 11158 (1998).

[7] J. R. Greer and W. D. Nix, Phys. Rev. B **73**, 245410 (2006).

[8] Z. W. Shan, R. K. Mishra, S. A. Syed Asif, O. L. Warren, and A. M. Minor, Nat. Mater. **7**, 115 (2008).

[9] M. D. Uchic, D. M. Dimiduk, J. N. Florando, and W. D. Nix, Science **305**, 986 (2004).

[10] D. M. Dimiduk, C. Woodward, R. LeSar, and M. D. Uchic, Science **312**, 1188 (2006).

[11] C. A. Volkert and E. T. Lilleodden, Philos. Mag. **86**, 5567 (2006).

[12] G. Rubio-Bollinger, S. R. Bahn, N. Agraït, K. W. Jacobsen, and S. Vieira, Phys. Rev. Lett. **87**, 026101 (2001).

[13] P. E. Marszalek, W. J. Greenleaf, H. Li, A. F. Oberhauser, and J. M. Fernandez, Proc. Natl. Acad. Sci. U.S.A. **97**, 6282 (2000).

[14] B. Wu, A. Heidelberg, J. J. Boland, J. E. Sader, X. M. Sun, and Y. D. Li, Nano Lett. **6**, 468 (2006).

[15] A. Gouldstone, N. Chollacoop, M. Dao, A. M. Minor, Ju Li, and Y.-L. Shen, Acta Mater. **55**, 4015 (2007).

[16] X. Li, H. Gao, C. J. Murphy, and K. K. Caswell, Nano Lett. **3**, 1495 (2003).

[17] G. Y. Jing, H. L. Duan, X. M. Sun, Z. S. Zhang, J. Xu, Y. D. Li, J. X. Wang, and D. P. Yu, Phys. Rev. B **73**, 235409 (2006).

[18] U. Landman, W. D. Luedtke, N. A. Burnham, and R. J. Colton, Science **248**, 454 (1990).

[19] J. Diao, K. Gall, and M. L. Dunn, Nat. Mater. **2**, 656 (2003).

[20] H. S. Park and J. A. Zimmerman, Phys. Rev. B **72**, 054106 (2005).

[21] D. Tabor, *Hardness of Metals* (Clarendon, Oxford, 1951).

[22] J. S. Field and M. V. Swain, J. Mater. Res. **10**, 101 (1995).

[23] S. Basu, A. Moseson, and M. W. Barsoum, J. Mater. Res. **21**, 2628 (2006).

[24] E. G. Herbert, G. M. Pharr, W. C. Oliver, B. N. Lucas, and J. L. Hay, Thin Solid Films **398-399**, 331 (2001).

[25] N. Iwashita, M. V. Swain, J. S. Field, N. Ohta, and S. Bitoh, Carbon **39**, 1525 (2001).

[26] S. Basu, M. W. Barsoum, A. D. Williams, and T. D. Moustakas, J. Appl. Phys. **101**, 083522 (2007).

[27] M. W. Barsoum, A. Murugaiah, S. R. Kalidindi, and T. Zhen, Phys. Rev. Lett. **92**, 255508 (2004).

[28] J. E. Sader, J. W. M. Chon, and P. Mulvaney, Rev. Sci. Instrum. **70**, 3967 (1999).

[29] M. S. Daw and M. I. Baskes, Phys. Rev. B **29**, 6443 (1984).

[30] M. S. Daw, S. M. Foiles, and M. I. Baskes, Mater. Sci. Rep. **9**, 251 (1993).

[31] A. F. Voter, Los Alamos National Laboratory Unclassified Technical Report No. LA-UR 93-3901, 1993 (unpublished).

[32] M. Zhou, Proc. R. Soc. London, Ser. A **459**, 2347 (2003).

[33] J. A. Zimmerman, E. B. Webb III, J. J. Hoyt, R. E. Jones, P. A. Klein, and D. J. Bammann, Modell. Simul. Mater. Sci. Eng. **12**, S319 (2004).

[34] E. T. Lilleodden and W. D. Nix, Acta Mater. **54**, 1583 (2006).

[35] S. G. Corcoran, R. J. Colton, E. T. Lilleodden, and W. W. Gerberich, Phys. Rev. B **55**, R16057 (1997).

[36] D. F. Bahr, D. E. Kramer, and W. W. Gerberich, Acta Mater. **46**, 3605 (1998).

[37] F. Milstein and S. Chantasiriwan, Phys. Rev. B **58**, 6006 (1998).